

Observation of the $I' \ ^1\Pi_g$ outer well state in H_2 and D_2

E. Reinhold, A. de Lange, W. Hogervorst, and W. Ubachs

Department of Physics and Astronomy, Vrije Universiteit, De Boelelaan 1081, 1081 HV Amsterdam, The Netherlands

(Received 20 July 1998; accepted 31 August 1998)

We observed bound levels of the I' state in H_2 and D_2 , confined in the outer well of the lowest $^1\Pi_g$ adiabatic potential close to its $(1s+2p)$ dissociation limit, with an equilibrium internuclear distance of ≈ 8 a.u. Rovibronic levels ($v=0-2$, $J=1-5$ for H_2 and $v=0-5$, $J=1-6$ for D_2) are populated with pulsed lasers in resonance enhanced XUV+IR (extreme ultraviolet+infrared) excitation, and probed by a third laser pulse. Level energies are measured with an accuracy of ≈ 0.03 cm^{-1} , and are in reasonable agreement with predictions from *ab initio* calculations in adiabatic approximation; the smallness of Λ -doublet splitting indicating that nonadiabatic interactions with $^1\Sigma_g^+$ states are generally weak. Additional resonances are observed close to the $n=2$ dissociation limit, some of which can be assigned as high vibrational levels of the $EF \ ^1\Sigma_g^+$ state. © 1998 American Institute of Physics. [S0021-9606(98)00246-3]

I. INTRODUCTION

The experimental investigation of excited singlet states of the hydrogen molecule has shown much progress in recent years with the application of multi-photon and extreme ultraviolet (XUV) laser spectroscopy.¹⁻⁹ These sophisticated techniques are presently employed to bridge the 11 eV gap between the ground state and the first excited singlet state in hydrogen and to drive transitions between excited states.

In contrast to singlet states of *ungerade* symmetry, for which spectral data were available from classical VUV absorption studies,¹⁰⁻¹² singlet *gerade* states do not have dipole-allowed transitions to the $X \ ^1\Sigma_g^+$ ground state. Therefore the excited *gerade* states were merely observed in discharges, where transitions between excited states may occur. These early studies resulted in a huge amount of spectral data, now tabulated in the form of *Dieke's atlas*.¹³ A traditional analysis of such emission spectra is difficult because of spectral congestion and because in a light molecule like hydrogen no simply assignable rotational band structures are formed. Moreover strong deviations from the Born-Oppenheimer approximation hamper a highly accurate theoretical description, so that even today a considerable fraction of the observed emission lines remain unassigned. A further motivation to investigate excited states of H_2 of the singlet *gerade* manifold is their possible role in visible wavelength absorptions in interstellar space, the diffuse interstellar bands (DIBs).^{14,15}

Selective excitation of a single quantum state using lasers opens the way to study transitions between excited states with well-defined quantum numbers. Subsequent multi-color excitation in double and multi-resonance schemes allows for probing transitions between excited states near the ionization and dissociation limits. The state-selectivity achieved by laser-based experiments, performed by our group⁹ and others,^{3,5,6,16} provides the necessary handle to unravel the complicated and perturbed structure of the excited singlet states in hydrogen.

Laser spectroscopy has led to the identification of most of the excited singlet states of the hydrogen molecule below the $H(n=1) + H(n=2)$ dissociation threshold, where levels are narrow in the absence of autoionization and predissociation. In the *ungerade* manifold, excitation of the highest vibrational $B \ ^1\Sigma_u^+$ levels, involving two-photon excitation to the $EF \ ^1\Sigma_g^+$ state and detection of higher excited levels by REMPI (resonance enhanced multi-photon ionization), revealed a perturbed level structure just below as well as above the dissociation limit.^{3,4,17} Investigation of *ungerade* Rydberg series allowed for a precise determination of the ionization energies of different isotopomers.¹⁸ Direct XUV excitation of the dissociation continuum of electronic *ungerade* states and detection of the fluorescence of the products by Balakrishnan *et al.* resulted in an accurate determination of the dissociation energy of the hydrogen molecule.^{1,19}

Tsukiyama and co-workers observed a number of singlet *gerade* levels close to the ($n=2$) limit using resonance-enhanced two-photon transitions, excited by XUV and visible pulsed lasers and detected by observation of their fluorescence in the visible and near infrared.^{2,16,20} Lifetimes were deduced from the exponential decay of the fluorescence. Chandler and Thorne²¹ employed a delayed laser pulse and REMPI detection to measure the decay times of some EF levels. Lifetimes of *gerade* states ($EF \ ^1\Sigma_g^+$, $H \ ^1\Sigma_g^+$, $I' \ ^1\Pi_g$, $J \ ^1\Delta_g$) were found to vary from about 10 to more than 100 ns, indicating that optical transitions between excited states is indeed the dominating decay mechanism, whereas XUV fluorescence to the $X \ ^1\Sigma_g^+$ or $b \ ^3\Sigma_u^+$ states is forbidden by dipole or spin selection rules.

In parallel to the experimental progress, *ab initio* calculations of the strongly interacting $^1\Sigma_g^+$, $^1\Pi_g$, and $^1\Delta_g$ systems have improved to agreement with observations within a few cm^{-1} , even for levels that are complicated superpositions of Born-Oppenheimer states with nonadiabatic shifts of more than 100 cm^{-1} .^{22,23} However, it appears that a number of predicted levels in the energy region close to the $n=2$ dissociation limit are still unobserved. At the one hand there

must exist higher vibrational levels of well-known electronic states; at the other, these calculations also predict a hitherto unobserved electronic state, called the I' state, which appears in the representation of adiabatic potentials as a shallow minimum of the $I'{}^1\Pi_g$ potential at large internuclear distance, separated from the known I state by a high barrier. We will refer to the two potential wells as I and I' states following Yu and Dressler,²³ calling the entire double-well potential II' .

The existence of a second, shallow well in the lowest ${}^1\Pi_g$ potential of the hydrogen molecule was first suggested by Mulliken²⁴ using the following argument. The long-range interaction of two hydrogen atoms in the lowest ${}^1\Pi_g$ -type superposition of the atomic orbitals $1s+2p$ is attractive;²⁵ the lowest ${}^1\Pi_g$ state of H_2 in the molecular-orbital basis is $1s\sigma_g3d\pi_g$, which is an $n=3$ Rydberg state with a potential distinctly above the $n=2$ dissociation limit at moderately large internuclear distance R . Due to the noncrossing rule, both must be connected at large R , forming a single adiabatic potential. The first calculation confirming the predicted outer potential minimum was performed by Browne.²⁶ It is not obvious whether the electronic configuration can be described more easily in terms of molecular orbitals (MO) or atomic orbitals (AO). In the MO basis, the I' potential well is formed by the core-excited $2p\sigma_u2p\pi_u$ electronic state, which is repulsive at small internuclear distance but correlates with the $1s\sigma_g3d\pi_g$ Rydberg potential via an avoided crossing, giving rise to a steep barrier. This is similar to the system of ${}^1\Sigma_g^+$ potentials, where the well-known double-well potential shapes are explained by molecular $1s\sigma_gn1\sigma_g$ orbitals of Rydberg states interacting with the doubly-excited $(2p\sigma_u)^2$ configuration; the EF potential as the lowest energy example is composed of a pure Rydberg state, forming the inner well, and a pure doubly-excited state that forms the outer well. In the AO basis, the I' minimum is explained by the interplay of the weak long-range dipole attraction with the repulsion due to the antibonding character of the $1s2p\pi{}^1\Pi_g$ Heitler-London configuration. Calculations by Browne,²⁶ and at higher accuracy by Zemke *et al.*²⁷ decide in favor of an atomic-orbital description, although major configuration mixing remains present. More recent *ab initio* calculations by Kołos and Rychlewski²⁸ (including also triplet and *ungerade* states) and by Dressler and Wolniewicz²⁹ start from a much larger set of basis functions, leading to an accurate potential over a wide range of internuclear distances. The I' state has a maximum binding energy of about 200 cm^{-1} at $R\approx 8$ a.u., which should sustain a couple of rovibronic levels whose energies are predicted in Ref. 29 for several isotopomers in the adiabatic approximation. Energies are given as part of a calculation of all levels in both wells of the II' potential; as the barrier at intermediate internuclear distance reaches a value of $\approx 1850\text{ cm}^{-1}$ above the dissociation energy, all levels are almost completely localized in either of the potential wells. So separate sets of vibrational quantum numbers are used for the I and I' states, following Yu and Dressler.²³

In the present study we report the observation of rovibrational I' levels in isotopomers of the hydrogen molecule, which are excited in XUV+IR two-photon transitions. Lev-

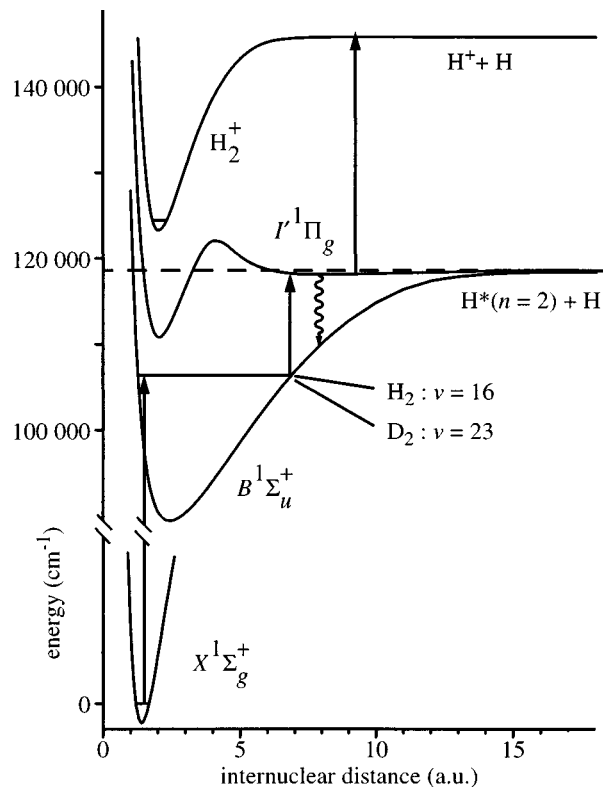


FIG. 1. Excitation scheme: $B{}^1\Sigma_u^+ - X{}^1\Sigma_g^+$ and $I'{}^1\Pi_g - B{}^1\Sigma_u^+$ transitions are driven by temporally overlapped XUV and IR laser pulses. A delayed probe pulse produces H^+ (or D^+) from excited I' levels by dissociative ionization.

els with $v=0-2$, $J=1-5$ in H_2 and with $v=0-5$, $J=1-6$ in D_2 of both (*e*) and (*f*) electronic symmetry are identified and their energies are determined, showing reasonable agreement with the *ab initio* calculations.²⁹ Some extra lines are found, which belong to transitions to EF and $GK{}^1\Sigma_g^+$ levels, and additionally some more complicated structure is observed in the vicinity of the ($n=2$) dissociation limit.

II. EXPERIMENT

The $I'{}^1\Pi_g$ levels in H_2 and D_2 are excited by two synchronous laser pulses in the XUV (extreme ultraviolet) and IR (infrared), driving a resonance-enhanced two-photon transition with a vibrational level of the $B{}^1\Sigma_u^+$ state as intermediate as illustrated in Fig. 1. Starting from a thermally populated rotational level with $v=0$ of the electronic ground state, a moderately high vibrational B level is excited, which is chosen to have good Franck-Condon overlap with the ground state and with the I' state around the inner and the outer classical turning point, respectively.

The general features of the experimental setup are similar to the one used for the investigation of the $H\bar{H}{}^1\Sigma_g^+$ state in H_2 .⁹ A schematic overview is given in Fig. 2. The output of a pulsed dye laser (PDL), pumped by the second harmonic of an injection seeded, Q-switched Nd:YAG laser, is frequency doubled in a KDP crystal, providing $\approx 35\text{ mJ/pulse}$ of coherent UV radiation. XUV radiation is produced via third harmonic generation from the UV beam, which is fo-

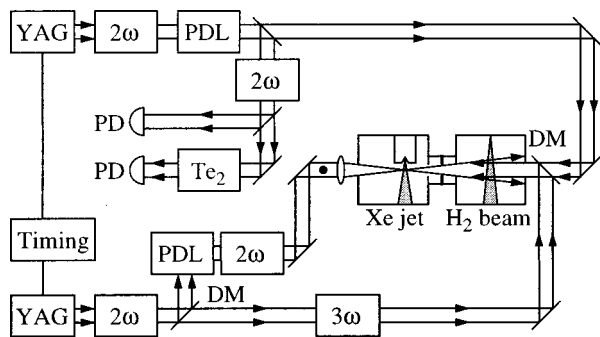


FIG. 2. Schematic experimental setup. PDL: pulsed dye laser. 2ω : second harmonic generation. 3ω : third harmonic generation. DM: dichroic mirror. PD: photo diode. The pulsed xenon jet and the collimated H_2 -beam flow in differentially pumped vacuum chambers.

cused ($f=18$ cm) in a pulsed jet of xenon. The tunable XUV light is tuned on and fixed to transitions from the $X^1\Sigma_g^+$ electronic ground state to selected rovibrational levels of the $B^1\Sigma_u^+$ state. The light for the second step, inducing transitions in the $I'-B$ system, is obtained from a second Nd:YAG pumped PDL.

There are different constraints for the choice of the vibrational B level, which determines the combination of wavelengths needed in both excitation steps: primarily the Franck-Condon overlap in the $I'-B$ system, but also the ease of generating XUV and IR and the possibility of a wavelength calibration of the second excitation step. The yield of XUV photons and the reliability of the XUV generation is best for $\lambda > 91$ nm; these wavelengths can be generated using the efficient and very stable dyes Rhodamine 6G and Fluorescein 27, pumped at high power by the second harmonic of a Nd:YAG laser (600 mJ at 532 nm). For the infrared wavelengths the LDS 925 dye combines a sufficient quantum efficiency (6%) in a wide range of wavelengths (900–940 nm) with solvability in methanol, such that the hazardous use of highly toxic solvents can be avoided. With these combinations of dyes, the rovibrational levels of the $B^1\Sigma_u^+$ state with $v=16$ in H_2 and $v=23$ in D_2 can be excited and the entire manifold of vibrational I' levels can be covered, while the Franck-Condon overlap in the $I'-B$ system is reasonable for both isotopes.

Since photons of the third harmonic of Nd:YAG (355 nm) are sufficiently energetic for dissociative ionization of a H_2 (or D_2) molecule from the I' state, but not from the B state, detection of H^+ ions can be used to record spectra of the $I'^1\Pi_g - B^1\Sigma_u^+$ band system. The ions are extracted from the interaction region by a pulsed electric field, which is delayed with respect to the laser pulses. Ions are mass-selected in a field-free time of flight (TOF) tube and collected at an electron multiplier. The signal from the electron multiplier is integrated by two boxcar integrators having the timing windows set for H^+ and H_2^+ ions. The IR and 355 nm beams are spatially overlapped by means of a dichroic mirror and both beams are then overlapped with the counterpropagating XUV beam, intersecting the molecular beam in the interaction region. The IR and the XUV beams are also temporally overlapped as the lifetime of the B state is ≈ 1 ns.

Apart from the H^+ signal ions produced via excitation of

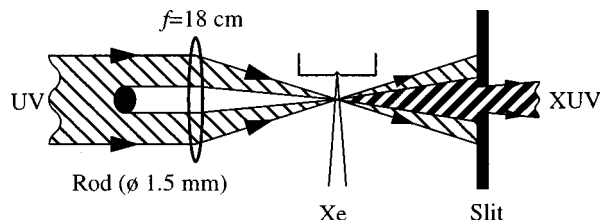


FIG. 3. The spectral filter separating the third harmonic XUV from the fundamental UV radiation. The rod creates a shadow in the UV distribution along the optical axis. A considerable fraction of the XUV is generated close to the axis and passes through the slit, which cuts off the UV.

the I' state also some parasitic H^+ and H_2^+ ions are produced by the combination of laser pulses. The energies of the XUV (≈ 93 nm) and fundamental UV (≈ 280 nm) photons are sufficient to produce H_2^+ ions in a REMPI process when the XUV is tuned in resonance with the B state. H^+ is also detected, originating from at least a three photon process; this phenomenon was discussed in Ref. 8. By separating the incident UV beam from the generated XUV, these background signals can be strongly reduced. The procedure and tools to geometrically separate the fundamental from the third harmonic are schematically displayed in Fig. 3. A rod (diameter $d=1.5$ mm) is placed in the UV beam ($d \approx 8$ mm), in front of the lens along the propagation of the overlapping light beams. A slit with adjustable central position and width is then used at a distance of ≈ 10 cm behind the focus to block the propagating UV-beam. The XUV-beam, predominantly generated on axis, due to phase-matching, is transmitted into the interaction region in the far field through the slit opening. The XUV-yield with this wavelength-separation setup is 40% of that obtained without XUV-UV separation.³⁰

Since the rovibronic energy levels of the $B^1\Sigma_u^+$ state are known,^{8,11} only the infrared used in the second excitation step needs to be calibrated for a determination of $I'^1\Pi_g$ level energies. Because no convenient reference-standard is available around 925 nm, part of the IR-light is frequency doubled in a KDP crystal, and a Te_2 -absorption spectrum (at 510 °C) is recorded simultaneously with the double resonance spectra probing the I' states. By fitting of the Te_2 -resonances with Gaussian profiles and assigning the peak positions with the Te_2 -atlas,³¹ an accurate frequency scale is constructed for the IR. Frequencies of the H_2 and D_2 lines are then determined via fitting of the resonances and comparison with the frequency scale. At low excitation intensities the linewidth of the H_2 and D_2 lines is about 0.08 cm^{-1} (FWHM), which corresponds to the IR laser linewidth. Because the molecular beam and the laser beams intersect perpendicularly residual Doppler broadening of the lines is negligible.

The spectra are recorded in two stages. First a series of overview spectra are measured, scanning the infrared dye with a step size of ≈ 0.05 cm^{-1} . Although this nearly equals the laser linewidth, all ($I'-B$) transitions are unambiguously discernible because the intensity of the infrared (≈ 2 mJ/pulse) is high enough to cause strong saturation broadening of the lines.

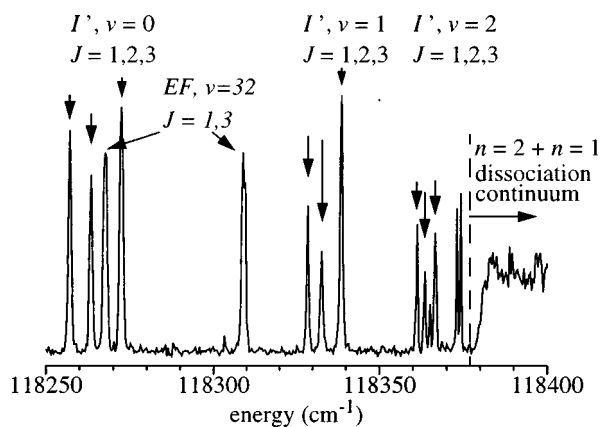


FIG. 4. XUV+IR spectrum of H_2 with the XUV laser tuned on the $B-X$ (16,0) $R(1)$ transition.

All transitions found in the overview spectra are next recorded a second time with a step size of 0.01 cm^{-1} , averaging over eight pulses per step to increase the signal/noise ratio. To prevent saturation broadening in these scans, the IR pulses are attenuated to $0.4 \mu\text{J}$ – 0.5 mJ , depending on transition strengths.

Figure 4 and the upper trace of Fig. 5 show typical spectra of H_2 and D_2 , displaying the H^+ and D^+ yield during an overview scan of the IR laser at full intensity, while the XUV frequency is fixed to the $B-X$ (16,0) $R(1)$ transition in H_2 and to $B-X$ (23,0) $R(3)$ in D_2 . Groups of three lines each can be discerned, which can easily be interpreted as the P , Q , and R transitions of one $I'-B$ (v',v) band; some additional lines are found in between. At energies beyond the $(n=1)+(n=2)$ dissociation limit, fragment atoms are ionized and detected. The lower trace of Fig. 5 shows the D^+ signal in a slow scan of the attenuated IR laser, resulting in laser limited linewidths, together with the Te_2 absorption spectrum.

III. RESULTS AND DISCUSSION

All observed transitions are listed in Table I for H_2 and in Table II for D_2 , with their assignments as discussed below. The question arises if the observed $I'-B$ ($v',v=16$) transitions in H_2 can be found in *Dieke's atlas*,¹³ which contains many unassigned emission lines in this wavelength range. Actually more than half of our observed transitions are found to nearly coincide (within estimated uncertainty margins), but these may be happenstance coincidences. Therefore a check for combination differences was made for transitions from the same upper levels to several B , $v \geq 16$ states, assuming that Frank-Condon factors are comparable in view of the potential shapes and the location of the classical turning points. In most cases no transitions at the predicted frequencies were found; we conclude that the $I'-B$ band system is probably not contained in *Dieke's atlas*.

Total level energies with respect to the ground state are obtained by adding the measured transition energies in the IR to the energies of the intermediate B levels; the latter were obtained by adding $B-X$ ($v',v=0$) transition energies from Ref. 8 and ground state rotational energies from Ref. 32 (H_2)

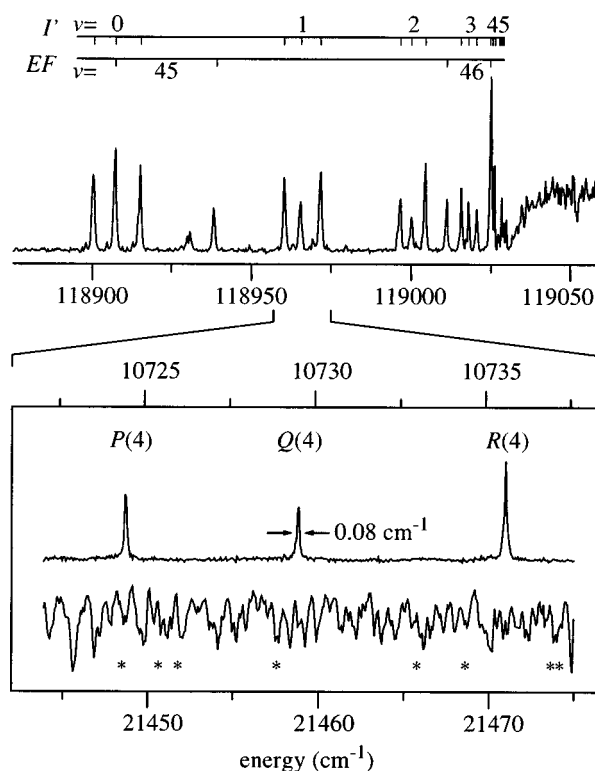


FIG. 5. XUV + IR spectrum of D_2 with the XUV laser tuned on the $B-X$ (23,0) $R(3)$ transition. Upper panel: overview scan, taken with $\approx 2 \text{ mJ}$ IR, with saturation broadened lines; on the abscissa the excitation energy (in cm^{-1}) with respect to the ground state. Lower panel: high resolution spectrum, registered with reduced IR intensity, showing the $I'-B$ (1,23) band transitions on the scale of transition energy, together with the Te_2 absorption spectrum of frequency doubled IR; lines marked with an asterisk are used for calibration.

and Ref. 33 (D_2). However, the present double resonance spectra allow for an improved determination of B state level energies because we observed many of the upper levels in P as well as R transitions, providing an extra check of combination differences. These have to be analyzed separately for systems of ortho and para levels, which are not interconnected by optical transitions. In H_2 , five cases of combination differences between intermediate levels with odd J are analyzed; they are consistent within the experimental uncertainty of the B level energies of $\approx 0.04 \text{ cm}^{-1}$ in Ref. 8, but some improvement is achieved by shifting the $J=1$ energy down by 0.01 cm^{-1} and the $J=3$ energy up by the same amount. For even J it turns out that combination differences of transitions via B , $v=16$, $J=2$ and 0 (five cases) are consistent within 0.02 cm^{-1} , while transitions via $J=4$, compared to $J=2$, give energies systematically lower by 0.1 cm^{-1} (four cases). We assume that the $J=4$ energy should be 0.1 cm^{-1} higher than derived from Ref. 8, but consistent with Ref. 12; this discrepancy is acceptable because in Ref. 8 the value is only based on the relatively weak $R(3)$ transition, while $J=0$ and 2 energies are consistently derived from the $P(1)$, $R(1)$ and $P(3)$ transitions. A similar analysis of combination differences in D_2 leads us to the assumption of B level energies that also differ slightly from values in Ref. 8. Level energies of the intermediate levels both for H_2 and D_2 as used to determine the excited state energies are listed

TABLE I. Transition energies in cm^{-1} in the second excitation step in H_2 with $B^1\Sigma_g^+$, $v=16$, J intermediate levels.

E	State	J'	E	State	J'	E	State	J'
via $B (J=0)$			via $B (J=1)$			via $B (J=3)$		
10679.45	$EF\ 31$	1	10680.09	$EF\ 31$	2	10567.32	$EF\ 31$	2
873.21	$I'\ 0$	1	853.02	$I'\ 0$	1	643.45	$EF\ 31$	4
883.60	$EF\ 32$	1	853.53	$EF\ 32$	0	749.63	$I\ 3$	4
944.58	$I'\ 1$	1	859.13	$I'\ 0$	2	755.37	$I'\ 0$	2
977.25	$I'\ 2$	1	881.38	$EF\ 32$	2	764.70	$I'\ 0$	3
989.19	a	1	924.36	$I'\ 1$	1	776.55	$I'\ 0$	4
via $B (J=2)$			928.48	$I'\ 1$	2	777.62	$EF\ 32$	2
			951.32	$GK\ 8$	0	794.64	b	
			957.00	$I'\ 2$	1	807.68	b	
10664.85	b		959.30	$I'\ 2$	2	824.67	$I'\ 1$	2
665.36	$EF\ 31$	3	970.02	b		828.66	$EF\ 32$	4
693.16	$I'\ 0$	4	972.54	b		830.86	$I'\ 1$	3
694.09	$I\ 3$	3	via $B (J=4)$			838.54	$I'\ 1$	4
811.75	$I'\ 0$	1				855.53	$I'\ 2$	2
818.01	$I'\ 0$	2				858.90	$I'\ 2$	3
822.16	$EF\ 32$	1	10609.65	$EF\ 31$	5	862.72	$I'\ 2$	4
827.04	$I'\ 0$	3	680.87	$I'\ 0$	3	866.23	b	
863.79	$EF\ 32$	3	664.95	b		867.66	b	
915.80	$I'\ 2$	1	707.46	$I'\ 0$	5	868.74	b	
918.14	$I'\ 2$	2	717.62	$EF\ 32$	3			
919.71	$GK\ 8$	1	747.12	$I'\ 1$	3			
921.33	$I'\ 2$	3	755.10	$I'\ 1$	4			
927.73	a	1	760.26	$EF\ 32$	5			
928.84	b		763.90	$I'\ 1$	5			
931.20	b		775.14	$I'\ 2$	3			
			779.24	$I'\ 2$	4			
			783.26	$I'\ 2$	5			

^aNo electronic and v assignment, but J assigned from combination differences.

^bAs (a), J' unknown between $J-1$ and $J+1$.

in Table III, together with the shifts with respect to Ref. 8 as well as the deviation from Ref. 12 for H_2 .

Unambiguous assignment of rovibrational $I' \ ^1\Pi_g$ levels is possible for $v=0-2$, $J=1-5$ (e electronic parity) and $J=1-4$ (f parity) in H_2 , and $v=0-5$, $J=1-6$ (e) and $J=1-5$ (f) in D_2 . Total energies of these levels with respect to the $X^1\Sigma_g^+$, $v=0$, $J=0$ ground state in each isotope are listed in Tables IV and VI and compared with *ab initio* values. Further levels that were observed are listed in Tables V and VII; their assignments are discussed below.

Theoretical I' level energies are derived from the most recent *ab initio* calculation by Dressler and Wolniewicz,²⁹ who give binding energies with respect to the $(n=2)+(n=1)$ dissociation limit. Energies with respect to the ground state are deduced by subtracting them from 118377.023 cm^{-1} for H_2 and 119029.700 cm^{-1} for D_2 ; these values follow from the sum of the most accurate dissociation energies of the respective ground state calculated by Wolniewicz³⁴ (36118.069 cm^{-1} for H_2 , 36748.364 cm^{-1} for D_2) and the $1s-2s$ atomic transition energy (82258.954 cm^{-1} for H_2 (Ref. 35) and 82291.336 cm^{-1} for D_2 (Ref. 36)). The calculation in Ref. 29 was made in the adiabatic approximation, so Λ -doublet levels are degenerate. However, nonadiabatic interaction with the manifold of $^1\Sigma_g^+$ states only occurs with (e) levels of $I' \ ^1\Pi_g$, resulting in a Λ -doublet splitting between (e) and (f) levels. In our excitation scheme with a $B^1\Sigma_u^+$ state as intermediate, (e) levels are

excited by P and R and (f) levels by Q transitions. The agreement between observed and calculated energies is very good for $v=0$ in H_2 as well as in D_2 (within $\approx 0.1 \text{ cm}^{-1}$ for both (e) and (f) levels), but deteriorates at higher v ; when interpreted as a relative deviation of binding energies (with respect to the dissociation limit), the discrepancy increases to as much as 25% for the highest observed vibrational level ($v=5$) in D_2 . This suggests that the *ab initio* calculation of the potential²⁹ is rather accurate for internuclear distances up to ≈ 10 a.u., but deviates in the long range region, where the highest vibrational wave functions typically have their largest amplitude.

Identification of the transitions that do not belong to the $I'-B$ system is somewhat more difficult, because nonadiabatic interactions are known to play a major role for states that are associated with potentials at short internuclear distance. Transitions in H_2 can be assigned as $EF-B$ and $GK-B$ with upper levels first identified by Tsukiyama *et al.*² as $EF^1\Sigma_g^+$, $v=31-32$ and $GK^1\Sigma_g^+$, $v=8$. Our results are consistent with Ref. 2 within the experimental uncertainty, except for EF , $v=31$, $J=4$, which is 0.3 cm^{-1} off as shown in Table V. Observed energies are about 60 cm^{-1} lower than calculated adiabatic energies³⁷ and still more than 20 cm^{-1} lower than first calculations taking nonadiabatic interactions into account,²² in the most recent *ab initio* calculation²³ the remaining discrepancy is only $\approx 3 \text{ cm}^{-1}$. A series of levels in D_2 appear to form two rotational progres-

TABLE II. Transition energies in cm^{-1} in the second excitation step in D_2 with $B^1\Sigma_u^+$, $v=23$, J intermediate levels.

E	State	J'	E	State	J'	E	State	J'
via $B (J=0)$			via $B (J=2)$			via $B (J=3)$		
10897.83	$I' 5$	1	10730.27	$EF 45$	1	10703.15	$I' 0$	2
899.55	a	1	731.92	$I' 0$	1	704.88	$EF 45$	2
			735.20	$I' 0$	2	708.04	$I' 0$	3
via $B (J=1)$			740.06	$I' 0$	3	714.48	$I' 0$	4
			746.74	$EF 45$	3	727.72	$EF 45$	4
10748.27	$EF 45$	0	792.61	$I' 1$	1	763.11	$I' 1$	2
753.27	$I' 0$	1	795.19	$I' 1$	2	766.97	$I' 1$	3
756.54	$I' 0$	2	798.96	$I' 1$	3	771.92	$I' 1$	4
758.28	$EF 45$	2	830.24	$I' 2$	1	800.04	$I' 2$	2
714.00	$I' 1$	1	832.07	$I' 2$	2	802.82	$I' 2$	3
816.53	$I' 1$	2	834.78	$I' 2$	3	806.26	$I' 2$	4
851.58	$I' 2$	1	839.62	$EF 46$	1	811.79	$EF 46$	2
853.41	$I' 2$	2	849.41	$EF 46$	3	820.15	$I' 3$	2
858.53	$EF 46$	0	850.95	$I' 3$	1	821.94	$I' 3$	3
865.12	$EF 46$	2	852.19	$I' 3$	2	824.48	$EF 46$	4
872.31	$I' 3$	1	853.96	$I' 3$	3	829.91	$I' 4$	2
873.52	$I' 3$	2	861.24	$I' 4$	1	830.96	$I' 4$	3
882.58	$I' 4$	1	861.97	$I' 4$	2	832.24	$I' 4$	4
883.30	$I' 4$	2	862.99	$I' 4$	3	834.15	$I' 5$	2
887.15	$I' 5$	1	865.78	$I' 5$	1	834.69	$I' 5$	3
887.53	$I' 5$	2	866.15	$I' 5$	2	835.31	$I' 5$	4
888.90	a	2	866.68	$I' 5$	3	835.64	a	2
889.06	a	2						
via $B (J=4)$			via $B (J=5)$			via $B (J=6)$		
10665.40	$I' 0$	3	10618.73	$I' 0$	4	10667.55	$I' 3$	5
671.92	$I' 0$	4	626.80	$I' 0$	5	670.63	$I' 3$	6
672.10	$EF 45$	3	632.00	$EF 45$	4	671.97	$EF 46$	5
679.73	$I' 0$	5	636.09	$I' 0$	6	673.56	$I' 3$	7
702.53	$EF 45$	5	664.47	$EF 45$	6	675.98	$I' 4$	6
724.33	$I' 1$	3	676.20	$I' 1$	4	676.69	$I' 5$	5
729.39	$I' 1$	4	682.43	$I' 1$	5	678.74	a	5
735.47	$I' 1$	5	689.45	$I' 1$	6			
760.15	$I' 2$	3	710.56	$I' 2$	4			
763.73	$I' 2$	4	714.92	$I' 2$	5			
767.97	$I' 2$	5	719.77	$I' 2$	6			
774.81	$EF 46$	3	728.06	$I' 3$	4			
779.32	$I' 3$	3	731.15	$I' 3$	5			
781.58	$I' 3$	4	734.00	$I' 3$	6			
784.18	$I' 3$	5	736.51	$I' 4$	4			
788.36	$I' 4$	3	737.98	$I' 4$	5			
788.57	$EF 46$	5	739.39	$I' 4$	6			
789.69	$I' 4$	4	739.57	$I' 5$	4			
791.08	$I' 4$	5	742.60	b				
792.06	$I' 5$	3						
792.69	$I' 5$	4						
793.30	$I' 5$	5						
795.32	a	5						

^aNo electronic and v assignment, but J assigned from combination differences.

^bAs (a), J' unknown between $J-1$ and $J+1$.

sions, to our knowledge hitherto unobserved; further analysis leads to an unambiguous assignment as EF vibrational levels.

A rotational analysis is performed for each observed vibrational level of the I' and EF states. For I' , energies of (e) and (f) rotational levels are simultaneously fitted to the formula

$$E_{vJ(f)} = \nu_v + B_v[J(J+1) - \Lambda^2] - D_v[J(J+1) - \Lambda^2]^2, \quad (1)$$

$$E_{vJ(e)} = E_{vJ(f)} + Q_v J(J+1). \quad (2)$$

Resulting parameters for H_2 and D_2 are listed in Table VIII. The rotational distortion constants D are large, indicating a strong deviation from a rigid rotator system; this is illustrated in Fig. 6 by a plot of energy vs $J(J+1)$ for levels in D_2 . For the EF state, the relation for Σ states is used,

$$E_{vJ} = \nu_v + B_v[J(J+1)] - D_v[J(J+1)]^2. \quad (3)$$

TABLE III. Energies of $B^1\Sigma_u^+$, $v=16$, J levels in H_2 and $v=23$, J levels in D_2 relative to the $X^1\Sigma_g^+$, $v=0$, $J=0$ ground state, corrected by the analysis of combination differences as explained in the text. Δ_1 refers to the correction with respect to Ref. 8 and Δ_2 to the difference from energies in Ref. 12 for H_2 . All values in cm^{-1} .

J	E_{obs}	Δ_1	Δ_2	E_{obs}	Δ_1
H ₂ : B , $v=16$					
0	107383.99	0.00	-0.08	108129.80	-0.02
1	107404.17	-0.01	+0.01	108140.46	-0.06
2	107445.44	0.00	-0.01	108161.84	-0.02
3	107507.94	+0.01	-0.01	108193.83	-0.01
4	107591.62	+0.10	+0.02	108236.46	+0.05
5				108289.56	0.00
6				108353.11	+0.18

The two unknown bands in D_2 can now be identified by comparing the results from the rotational analysis with predictions for some vibrational levels of *gerade* states from Ref. 37; expectation values $\langle R^{-2} \rangle$ of adiabatic vibrational wave functions in the nonrotating molecule are converted into B constants by the relation

$$B = \frac{\hbar}{4\pi c \mu} \langle R^{-2} \rangle \quad (4)$$

(B constants in cm^{-1} ; molecular reduced mass $\mu = 918.0764 m_e$ for H_2 and $1835.2395 m_e$ for D_2). The empirical ν and B constants (1.704 and 1.084 cm^{-1} ; cf. Table VIII) are consistent with theoretical values of $\nu = 44-46$ levels (2.074 , 1.581 , and 0.632 cm^{-1}).³⁷ The assignments are tentatively EF , $v=45$ and 46 assuming that deviations between observed levels and adiabatic calculation are similar in H_2 and D_2 ; further confirmation is obtained from the predicted energy of the $v=45$, $J=5$ level in Ref. 23, Table VIII, which is only $\approx 4 \text{ cm}^{-1}$ higher than the experimental value.

The observed Λ -doublet splittings in the $I'^1\Pi_g$ state are generally very small ($\ll 1 \text{ cm}^{-1}$); the Q constants in Eq. 2 reflect the systematic shift of the (e) levels caused by their heterogeneous, nonadiabatic interaction with states of the $^1\Sigma_g^+$ manifold. This includes contributions from bound vibrational levels that lie far away in energy, as well as from the dissociation continuum of these states. Possible systematic shifts caused by states with $\Lambda \geq 1$ are not accounted for because they affect (e) and (f) levels identically. However, near coincidence with a rovibrational level of another electronic state may cause a distortion.

The values Q_v obtained from the fit are only marginally significant in view of the derived uncertainties, with (e) levels lying slightly lower than (f) levels; however, in D_2 one example of a resonant nonadiabatic interaction is found that provides some information on the coupling strength of the I' state with other states: The $J=4$ levels of the $I'^1\Pi_g(e)$, $v=3$ and the $EF^1\Sigma_g^+$, $v=46$ states coincide in the rotational analysis; in the experiment the levels are found to be separated by 0.6 cm^{-1} (cf. Fig. 6), while for other J levels no significant deviation from the rotational fit is found. The underlying interaction is analyzed by invoking a heterogeneous

TABLE IV. Energies of the $I'^1\Pi_g$ levels in H_2 relative to the $X^1\Sigma_g^+$, $v=0$, $J=0$ ground state. E_{calc} values are derived from binding energies given in Ref. 29, shifted appropriately on the energy scale as explained in the text. All values in cm^{-1} .

J	E_{calc}	(e) levels		(f) levels	
		E_{obs}	Δ_{oc}	E_{obs}	Δ_{oc}
$v=0$					
1	118257.17	118257.20	+0.03	118257.19	+0.02
2	118263.40	118263.31	-0.09	118263.45	+0.05
3	118272.63	118272.48	-0.15	118272.64	+0.01
4	118284.72	118284.49	-0.23	118284.78	+0.06
5	118299.46	118299.08	-0.38		
$v=1$					
1	118328.13	118328.58	+0.45	118328.53	+0.40
2	118332.29	118332.64	+0.35	118332.80	+0.51
3	118338.35	118338.74	+0.39	118338.79	+0.44
4	118346.10	118346.48	+0.38	118346.72	+0.62
5	118355.19	118355.52	+0.33		
$v=2$					
1	118360.13	118361.24	+1.11	118361.17	+1.04
2	118362.48	118363.47	+0.99	118363.58	+1.10
3	118365.80	118366.76	+0.96	118366.84	+1.04
4	118369.82	118370.66	+0.84	118370.86	+1.04
5	118374.12	118374.88	+0.76		

(J -dependent) coupling between the I' , $v=3$ and EF , $v=46$ vibrational states and solving the eigenvalue problem for each value of J ,

$$\begin{pmatrix} E_{I'(3)} & \eta\sqrt{J(J+1)} \\ \eta\sqrt{J(J+1)} & E_{EF(46)} \end{pmatrix} \Psi = E\Psi. \quad (5)$$

From the fit to the observed level energies a coupling constant of $\eta = 0.077(4) \text{ cm}^{-1}$ is determined. The two $J=4$ eigenstates have mixed I' and EF character of nearly equal contribution, while all other J states turn out to be pure states, with less than 1% admixture of the other electronic character. In H_2 no such strong mixture of I' and other states was found.

The energies of the I' levels and the interaction with the EF state are accurately described by the relations in Eqs. (1), (2), and (5) with deviations of less than 0.05 cm^{-1} throughout. Thus it is found that nonadiabatic effects in the I' outerwell state appear to be small; the adiabatic approximation used in the calculation in Ref. 29 seems to be valid. It is known, in contrast, that nonadiabatic effects do play an important role at shorter internuclear distances, where large Λ -doublet splittings are reported for all rotational levels. Heterogeneous interaction between states with different Λ within the singlet *gerade* manifold is attributed to the rotational coupling between the Rydberg states of the $3d$ complex, $(3d\sigma)G^1\Sigma_g^+$, $(3d\pi)I^1\Pi_g$ and $(3d\delta)J^1\Delta_g$. The situation is complicated by homogeneous interaction between the $^1\Sigma_g^+$ states, which stems from the crossing of $(1s\sigma_g n l \sigma_u)$ Rydberg state potentials with the doubly excited $(2p\sigma_u)^2$ configuration.²² So it is not surprising that the representation of EF levels by a rotational progression [cf. Eq. (3)] is less accurate, because (in contrast to the I' state) the

TABLE V. Energies of identified EF , $GK^1\Sigma_g^+$ and $I^1\Pi_g$ levels in H_2 ; Δ_1 is the difference from values from Refs. 2, 23 and Δ_2 gives the deviation from a fit to Eq. (3) with constants listed in Table VIII.

J	E_{obs}	Δ_1	J	E_{obs}	Δ_1	Δ_2
$EF, v=31$			$EF, v=32$			
0	118052.99 ^a		0	118257.70	-0.01	-0.20
1	118063.44	-0.03	1	118267.59	-0.02	+0.17
2	118084.26	-0.05	2	118285.55	-0.07	+0.21
3	118110.80	0.00	3	118309.23	+0.02	-0.25
4	118151.39	-0.31	4	118336.60	-0.08	+0.07
5	118201.27	-0.02	5	118351.88	-0.01	-10.22 ^b
$GK, v=8$			$I, v=3(e)$			
0	118355.49	+0.04	3	118139.53	+0.17	
1	118365.15	-0.01	4	118257.57	-0.05	

^aValue taken from Ref. 2.^bLevel left out of the fit.

vibrational wave functions of these levels extend over a wide range of internuclear distance R and therefore interact with other states at small R .

In Tables V and VII deviations between observed energies of the EF levels and a fit to Eq. (3) are listed. The fits for the $EF, v=45$ and $v=46$ states in D_2 do not reproduce the $v=45, J=5$ and $v=46, J=0$ energies, which had to be left aside in the fitting procedure. Their deviations of $+2.29$ and -0.35 cm^{-1} , respectively are presumably due to the nonadiabatic interaction with near-coincident levels. For the former, we found a candidate perturber state which lies 7.68 cm^{-1} lower in energy.

The level energies of the $EF, v=31$ state in H_2 are strongly distorted, leading to deviations from a fit using Eq. (3) of more than 1 cm^{-1} for several levels; we do not present fit parameters because they are not meaningful. This situation is not unexpected, as the calculation of Yu and Dressler²³ shows that three rotational level progressions cross $EF, v=31$ between $J=2$ and 3 ($I^1\Pi_g, v=3$; $O^1\Sigma_g^+, v=0$; and $S^1\Delta_g, v=0$). The rotational fit of the $EF, v=32$ state represents the $J=0-4$ levels reasonably (cf. Table V); deviations in the order of 0.2 cm^{-1} are significant in view of the experimental uncertainty, indicative of perturbations. The observed energy if the $J=5$ level is 10 cm^{-1} lower than the fit; this striking feature is consistent with *ab initio* calculations within 3 cm^{-1} , Ref. 23.

Some transitions in both H_2 and D_2 still remain unassigned. The observation of a strong H^+ signal on these resonances close to the ($n=2$) dissociation threshold suggests that they are associated with bound levels stretching to the long range part of the potentials, but no obvious band structure is found. A similar perturbed structure close to the ($n=2$) dissociation limit was found earlier in the system of *ungerade* states, by Eyler and co-workers.^{3,4} The extra transitions were in a qualitative sense attributed to couplings between singlet and triplet, as well as between *ungerade* and *gerade* states close to the dissociation threshold. A detailed investigation of the perturbed structure in this energy range remains the subject of future work.

Ab initio calculations^{29,37} predict one more vibrational I' level in H_2 ($v=3$) and for both H_2 and D_2 in the EF state

TABLE VI. Energies of the $I'^1\Pi_g$ levels in D_2 relative to the $X^1\Sigma_g^+, v=0, J=0$ ground state. E_{calc} values are derived from Ref. 29 in the same way as for H_2 in Table IV. Unperturbed levels are represented by Eqs. (1) and (2) within 0.05 cm^{-1} .

J	E_{calc}	(e) levels			(f) levels	
		E_{obs}	Δ_{oc}	E_{obs}	Δ_{oc}	
$v=0$						
1	118893.68	118893.76	+0.08	118893.73	+0.05	
2	118896.95	118896.99	+0.04	118897.04	+0.09	
3	118901.84	118901.88	+0.04	118901.87	+0.03	
4	118908.30	118908.30	0.00	118908.38	+0.08	
5	118916.29	118916.19	-0.10	118916.36	+0.07	
6		118925.65				
$v=1$						
1	118954.26	118954.45	+0.19	118954.46	+0.20	
2	118956.82	118956.97	+0.15	118957.03	+0.21	
3	118960.62	118960.80	+0.18	118960.80	+0.18	
4	118965.63	118965.76	+0.13	118965.85	+0.22	
5	118971.77	118971.93	+0.16	118971.99	+0.22	
6		118979.01				
$v=2$						
1	118991.30	118992.08	+0.78	118992.04	+0.74	
2	118993.13	118993.87	+0.74	118993.91	+0.78	
3	118995.83	118996.60	+0.77	118996.65	+0.82	
4	118999.34	119000.11	+0.77	119000.19	+0.85	
5	119003.59	119004.43	+0.84	119004.48	+0.89	
6		119009.33				
$v=3$						
1	119011.66	119012.79	+1.13	119012.77	+1.11	
2	119012.88	119013.98	+1.10	119014.03	+1.15	
3	119014.65	119015.79	+1.14	119015.77	+1.12	
4	119016.93	119018.31	a	119018.04	+1.11	
5	119019.63	119020.65	+1.02	119020.71	+1.08	
6		119023.56		119023.74		
7		119026.67				
$v=4$						
1	119022.09	119023.08	+0.99	119023.04	+0.95	
2	119021.83	119023.76	+0.93	119023.81	+0.98	
3	119023.90	119024.83	+0.93	119024.79	+0.89	
4	119025.24	119026.07	+0.83	119026.15	+0.91	
5	119026.75	119027.54	+0.79	119027.54	+0.79	
6		119028.95				
$v=5$						
1	119026.95	119027.63	+0.68	119027.61	+0.66	
2	119027.38	119027.98	+0.60	119027.99	+0.61	
3	119027.99	119028.52	+0.53	119028.52	+0.53	
4		119029.14		119029.15		
5		119029.78	b			

^aPerturbed by $EF, v=46, J=4$.^bResonance above threshold.

($v=33$ and $v=47$ respectively). A further estimate can be obtained by an analysis of the number of vibrational states that are sustained by a potential close to its dissociation limit, following LeRoy and Bernstein³⁸ and Stwalley,³⁹ only the long-range behavior of the potential curve is needed as an input to extrapolate from the known vibrational level structure. There are three singlet *gerade* potentials in the hydrogen molecule that dissociate into $H(n=1)+H(n=2)$, the $EF^1\Sigma_g^+$, the $GK^1\Sigma_g^+$, and the $II'^1\Pi_g$ potentials, which correlate at large distance with atomic states $1s+2s$, $1s+2p\sigma$, and $1s+2p\pi$, respectively. The leading terms in the

TABLE VII. Energies of identified $EF\ ^1\Sigma_g^+$ levels in D_2 . Δ gives the deviation from a fit to Eq. (3) with constants listed in Table VIII. All values in cm^{-1} .

J	E_{obs}	Δ	J	E_{obs}	Δ
$EF, v=45$			$EF, v=46$		
0	118888.73	+0.06	0	118998.99	-0.35
1	118892.11	+0.03	1	119001.46	-0.02
2	118898.73	-0.08	2	119005.59	+0.02
3	118908.57	-0.11	3	119011.26	+0.02
4	118921.55	+0.12	4	119017.62	-0.03
5	118938.99	+2.29	5	119025.06	+0.01
6	118954.03	-0.02			

long-range potentials were calculated by Stephens and Dalgarno.⁴⁰ The I' state shows a dipole attraction $\propto R^{-3}$, while the EF state is attractive with a van der Waals potential $\propto R^{-6}$. So both these states might contain v levels close to the dissociation limit. The GK potential is repulsive $\propto R^{-3}$ in the long range, and shows a barrier of $\approx 100\text{ cm}^{-1}$ above the asymptotic energy at $R \approx 8\text{ a.u.}$,³⁷ so it can be left aside in the analysis.

According to LeRoy and Bernstein³⁸ and Stwalley,³⁹ the binding energies ε_v of vibrational levels v close to the dissociation limit of a potential that asymptotically follows a simple power law, $V = -C_n R^{-n}$, are related by

$$v_D - v \approx a_n \varepsilon_v^{(n-2)/2n} \quad (6)$$

with

$$a_n = \frac{2\sqrt{\pi}}{n-2} \frac{\Gamma(1/2+1/n)}{\Gamma(1+1/n)} \frac{\sqrt{2\mu}}{h} C_n^{1/n}, \quad (7)$$

derived from Eqs. (7) and (8) in Ref. 39; the constant v_D can be interpreted as the "effective" vibrational quantum number at the dissociation threshold. From experimental values of ε_v one can derive v_D by extrapolating to $\varepsilon_v = 0$ and determine binding energies of vibrational levels for integer val-

TABLE VIII. Results of the rotational analysis of vibrational levels in H_2 and D_2 according to Eqs. (1), (2); the interaction of $EF, v=46$ and $I', v=3$ is accounted for following Eq. (5). All values in cm^{-1} .

v	ν_v	B_v	$D_v/10^{-3}$	$Q_v/10^{-3}$
H ₂ : I' state				
0	118255.63	1.570	1.88	-16.3
1	118327.49	1.068	3.05	-12.7
2	118360.60	0.609	3.68	-10.2
H ₂ : EF state				
32	118257.90	4.85	46.	
D ₂ : I' state				
0	118892.93	0.821	0.46	-4.6
1	118953.80	0.647	0.70	-3.4
2	118991.59	0.467	0.76	-2.9
3	119012.47	0.309	0.91	-2.6
4	119022.86	0.190	0.97	-1.2
5	119027.51	0.099	0.71	-0.6
D ₂ : EF state				
45	118888.67	1.711	3.68	
46	118999.34	1.084	7.63	

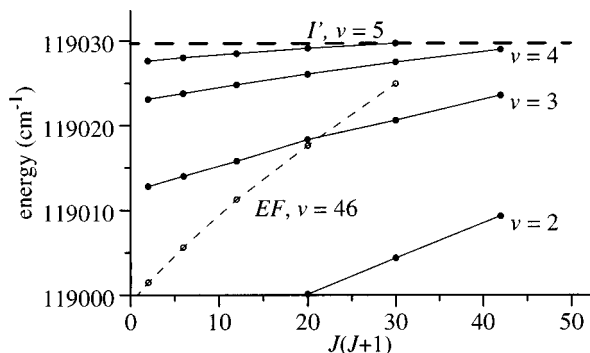


FIG. 6. Rovibronic energies of the highest observed $I'(e)$ and EF levels in D_2 as a function of $J(J+1)$; the deviation from a straight line indicates the strong nonrigidity of vibrational levels close to the dissociation threshold. The $I', v=3, J=4$ level is perturbed by $EF, v=46$.

ues $v \leq v_D$. For the I' potential, $n=3$ and $C_3=0.554929$ (in atomic units) from Ref. 40 lead to $a_3(H_2)=3.2343$ and $a_3(D_2)=4.5722$, with ε_v to be taken in cm^{-1} . Figure 7 shows a modified Birge-Sponer plot of $(v-v_D)/a_3$ against $\varepsilon_v^{1/6}$, which allows us to include experimental values of both isotopes in a single graph. ε_v is taken with respect to 118377.1 cm^{-1} for H_2 and 119029.7 cm^{-1} for D_2 ; the results discussed here are insensitive to an uncertainty of at least 0.2 cm^{-1} . We find that data points of both isotopes fit well to a straight line with a slope of -0.97 , close to the expected slope of -1 . Strikingly there is no deviation from linearity even for the lowest v levels. Extrapolation to $\varepsilon_v = 0$ leads to effective vibrational quantum numbers at the dissociation threshold of $v_D=6.99$ in H_2 and $v_D=10.10$ in D_2 . So in the adiabatic approximation, 4–5 more vibrational levels are expected above the identified ones in both isotopes; however, the highest ones are too close to the dissociation limit to be undisturbed by fine and hyperfine interaction. A similar analysis for the observed levels in the EF state, with $n=6$ in view of the van der Waals potential at large distance, shows strong deviation from the relation of Eq. (7). It follows that both in H_2 and D_2 , an additional vibrational level is expected at binding energies in the range $0.5\text{--}5\text{ cm}^{-1}$. This analysis holds for the nonrotating molecule ($J=0$); for all $J>0$ states the long-range potential is dominated by the (repulsive) centrifugal term $\mu J(J+1)/R^2$, effectively limiting the number of stable rotational levels. For the I' state there exist no $J=0$ levels, so at least $J=1$ has to be stable for a vibrational level to exist at all. The predicted binding energy of the $I', v=3$ state in H_2 is $\approx 4\text{ cm}^{-1}$, which is more than for the observed $v=5$ level in D_2 ; at least three J levels should be stable. However, an EF level ($v=33$) is expected at roughly the same energy, which probably interacts with the $I', v=3$ level. Indeed some levels are observed in this energy range with perturbed positions such that we cannot assign them.

Incidentally rotational levels which lie slightly above the dissociation energy are metastable, due to confinement by the centrifugal barrier; this phenomenon occurs in the $I', v=5, J=5$ state of the D_2 molecule (cf. Table VI), observed as a narrow resonance several 0.01 cm^{-1} above the dissociation threshold. The long-range potential for the $1s$

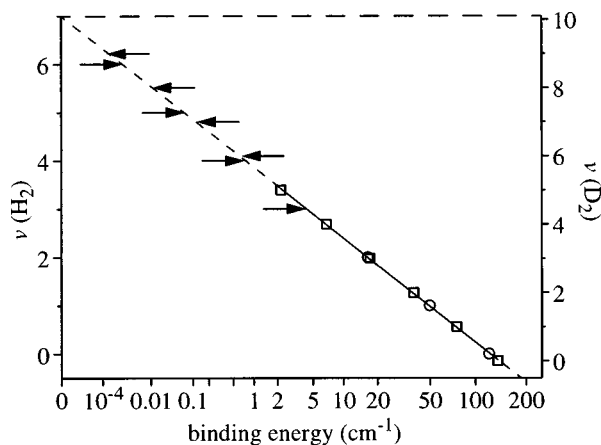


FIG. 7. Plot of the vibrational quantum number v of I' levels in H_2 (circles) and D_2 (squares) as function of the binding energy on an $\epsilon^{1/6}$ scale. v is taken on a $(v - v_D)/a_3$ scale to fit data points of both isotopes with a single straight line. Arrows indicate positions of predicted levels.

+ $2p\pi$ case⁴⁰ and the centrifugal potential for D_2 with $J = 5$ give rise to a barrier of $\approx 0.05 \text{ cm}^{-1}$ at an internuclear distance of 100 a.u. An estimate of the tunneling probability in the WKB approximation shows a very strong energy dependence (one order of magnitude per 0.01 cm^{-1}), so a quantitative prediction of the resonance width would require an extremely small energy uncertainty.

Figure 8 shows the onset of the $n=2$ dissociation continuum, excited from a $J=1$ intermediate level; thus continuum states with J between 0 and 2 may contribute. The delayed third laser pulse ionizes atoms left in the $2s$ state after dissociation; atoms in the $2p$ state are not detected due to their short lifetime. Wigner's threshold law implies that the yield as a function of excess energy ϵ is

$$I \propto \epsilon^{J+1/2}, \quad (8)$$

as pointed out in Ref. 4. This implies that the onset of the $J=0$ continuum is sharp. Although in Fig. 8 the threshold region is overlapped by the wing of a strongly saturation-broadened resonance, we can derive an approximate value of $118377.2 \pm 0.1 \text{ cm}^{-1}$ for the $1s+2s$ dissociation energy in the singlet *gerade* case, 0.14 cm^{-1} higher than the most accurate value found in the singlet *ungerade* system.^{1,19} Further studies are needed to investigate the complex system of different dissociation limits that arise from the fine and hyperfine splitting of the $n=1$ and $n=2$ states of the hydrogen atom.

IV. CONCLUSION

A large number of levels of the hitherto unobserved $I' \ ^1\Pi_g$ state of H_2 and D_2 were excited with a resonant two-photon laser excitation technique, applying pulsed XUV and IR radiation. Careful choice of the intermediate levels leads to good Franck-Condon overlap with the wave function confined in a shallow potential well at large internuclear distance, just below the second dissociation limit. Other levels were found in the same energy region, some of which were also observed for the first time and could be successfully identified. Nonadiabatic interactions of the I' levels with the

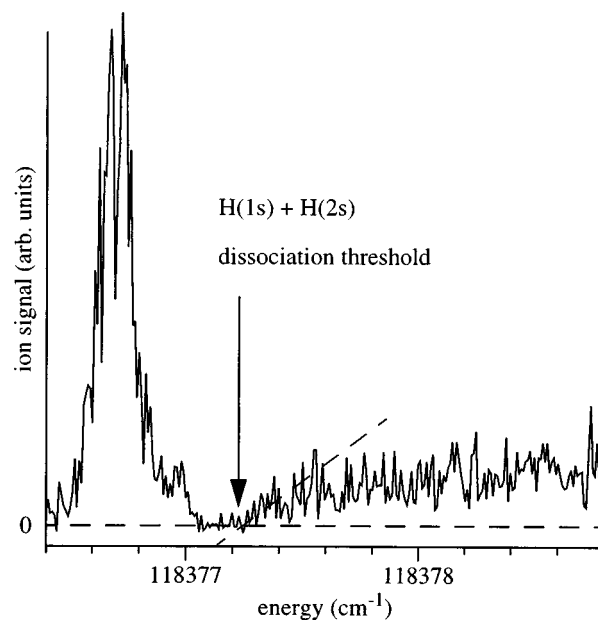


FIG. 8. H_2 dissociation spectrum excited from the $B \ ^1\Sigma_u^+, v=16, J=1$ state; $H(2s)$ fragments are probed by the H^+ signal that is produced by the delayed UV pulse. The sudden onset of dissociation at 118377.2 cm^{-1} , indicated by a dashed line as a guide to the eye, is attributed to the $J=0$ continuum.

other states were investigated, which can account for some irregularities in the I' spectrum. These interactions turn out to be about two orders of magnitude weaker than similar interactions between other *gerade* states of the hydrogen molecule. The same holds for the systematic interaction with the whole $^1\Sigma_g^+$ manifold as deduced from the small Λ -doublet splitting. Some spectral lines very close to the dissociation limit remain unassigned; a detailed investigation of the perturbed structure in this energy range remains the subject of future work.

ACKNOWLEDGMENTS

The authors wish to acknowledge The Netherlands Foundation for Fundamental Research on Matter (FOM) for financial support and the Vrije Universiteit for a special (USF) grant.

- ¹A. Balakrishnan, V. Smith, and B. P. Stoicheff, *Phys. Rev. Lett.* **68**, 2149 (1992).
- ²K. Tsukiyama, S. Shimizu, and T. Kasuya, *J. Mol. Spectrosc.* **155**, 325 (1992).
- ³E. F. McCormack and E. E. Eyler, *Phys. Rev. Lett.* **66**, 1042 (1991).
- ⁴E. E. Eyler and N. Melikechi, *Phys. Rev. A* **48**, R18 (1993).
- ⁵H. Rottke and K. H. Welge, *J. Chem. Phys.* **97**, 908 (1992).
- ⁶W. L. Glab and J. P. Hessler, *Phys. Rev. A* **35**, 2102 (1987).
- ⁷W. L. Glab, K. Qin, and J. Bistransin, *J. Chem. Phys.* **102**, 2338 (1994).
- ⁸P. C. Hinnen, W. Hogervorst, S. Stolte, and W. Ubachs, *Can. J. Phys.* **72**, 1032 (1994).
- ⁹E. Reinhold, W. Hogervorst, and W. Ubachs, *Phys. Rev. Lett.* **78**, 2543 (1997).
- ¹⁰I. Dabrowski and G. Herzberg, *Can. J. Phys.* **52**, 525 (1976).
- ¹¹I. Dabrowski, *Can. J. Phys.* **62**, 1639 (1984).
- ¹²H. Abgrall, E. Roueff, F. Launay, J.-Y. Roncin, and J.-L. Subtil, *J. Mol. Spectrosc.* **157**, 512 (1993).
- ¹³H. M. Crosswhite, *The Hydrogen Molecule Wavelength Tables of Gerhard Heinrich Dieke* (Wiley-Interscience, New York, 1972).
- ¹⁴P. P. Sorokin and J. Glowina, *Astrophys. J.* **473**, 900 (1996).

- ¹⁵W. Ubachs, P. C. Hinnen, and E. Reinhold, *Astrophys. J.* **476**, L93 (1997).
- ¹⁶K. Tsukiyama, J. Ishii, and T. Kasuya, *J. Chem. Phys.* **97**, 875 (1992).
- ¹⁷C. H. Cheng, J. T. Kim, E. E. Eyler, and N. Melikechi, *Phys. Rev. A* **57**, 949 (1998).
- ¹⁸J. M. Gilligan and E. E. Eyler, *Phys. Rev. A* **46**, 3676 (1992).
- ¹⁹A. Balakrishnan, V. Smith, and B. P. Stoicheff, *Phys. Rev. A* **49**, 2460 (1994).
- ²⁰J. Ishii, K. Tsukiyama, and K. Uehara, *Laser Chem.* **14**, 31 (1994).
- ²¹D. W. Chandler and L. R. Thorne, *J. Chem. Phys.* **85**, 1733 (1986).
- ²²P. Quadrelli, K. Dressler, and L. Wolniewicz, *J. Chem. Phys.* **92**, 7461 (1990).
- ²³S. Yu and K. Dressler, *J. Chem. Phys.* **101**, 7692 (1994).
- ²⁴R. S. Mulliken, *Phys. Rev.* **138**, A962 (1964).
- ²⁵J. C. Browne, *J. Chem. Phys.* **41**, 1583 (1964).
- ²⁶J. C. Browne, *Phys. Rev.* **138**, A9 (1965).
- ²⁷W. T. Zemke, P. G. Lykos, and A. C. Wahl, *J. Chem. Phys.* **51**, 5635 (1969).
- ²⁸W. Kołos and J. Rychlewski, *J. Mol. Spectrosc.* **66**, 428 (1977).
- ²⁹K. Dressler and L. Wolniewicz, *Can. J. Phys.* **62**, 1706 (1984).
- ³⁰P. C. Hinnen, Ph.D. thesis, Vrije Universiteit, Amsterdam, 1997.
- ³¹J. Cariou and P. Luc, *Atlas du spectre d'absorption de la molécule de tellure* (Orsay, France, 1980).
- ³²S. L. Bragg, J. W. Brault, and W. H. Smith, *Astrophys. J.* **263**, 999 (1982).
- ³³A. R. W. McKellar and T. Oka, *Can. J. Phys.* **56**, 1315 (1978).
- ³⁴L. Wolniewicz, *J. Chem. Phys.* **103**, 1792 (1995).
- ³⁵T. Udem, A. Huber, B. Gross, J. Reichert, M. Prevedelli, M. Weitz, and T. Hänsch, *Phys. Rev. Lett.* **79**, 2646 (1997).
- ³⁶M. G. Boshier, P. E. G. Baird, C. J. Foot, E. A. Hinds, M. D. Plimmer, D. N. Stacey, J. B. Swan, D. A. Tate, D. M. Warrington, and G. K. Woodgate, *Nature (London)* **330**, 463 (1987).
- ³⁷L. Wolniewicz and K. Dressler, *J. Chem. Phys.* **82**, 3292 (1985).
- ³⁸R. J. LeRoy and R. B. Bernstein, *J. Chem. Phys.* **52**, 3869 (1970).
- ³⁹W. C. Stwalley, *Chem. Phys. Lett.* **6**, 241 (1970).
- ⁴⁰T. L. Stephens and A. Dalgarno, *Mol. Phys.* **28**, 1049 (1974).